

PAPER • OPEN ACCESS

Terahertz absorption spectroscopy for measuring atomic oxygen densities in plasmas

To cite this article: J R Wubs *et al* 2023 *Plasma Sources Sci. Technol.* **32** 025006

View the [article online](#) for updates and enhancements.

You may also like

- [The role of thermal energy accommodation and atomic recombination probabilities in low pressure oxygen plasmas](#)
Andrew Robert Gibson, Mickaël Foucher, Daniil Marinov *et al.*
- [Atomic oxygen generation in atmospheric pressure RF plasma jets driven by tailored voltage waveforms in mixtures of He and O₂](#)
I Korolov, D Steuer, L Bischoff *et al.*
- [Two-photon absorption laser induced fluorescence measurement of atomic oxygen density in an atmospheric pressure air plasma jet](#)
J Conway, G S Gogna, C Gaman *et al.*



Analysis Solutions for your Plasma Research

- Knowledge
- Experience ■ Expertise

[Click to view our product catalogue](#)

Contact Hiden Analytical for further details:
W www.HidenAnalytical.com
E info@hiden.co.uk



Surface Science

- ▶ Surface Analysis
- ▶ SIMS



Surface Science

- ▶ 3D depth Profiling
- ▶ Nanometre depth resolution



Plasma Diagnostics

- ▶ Plasma characterisation
- ▶ Customised systems to suit plasma Configuration



Plasma Diagnostics

- ▶ Mass and energy analysis of plasma ions
- ▶ Characterisation of neutrals and radicals

Terahertz absorption spectroscopy for measuring atomic oxygen densities in plasmas

J R Wubs^{1,*} , U Macherius¹ , K-D Weltmann¹ , X Lü² , B Röben^{2,3} , K Biermann² , L Schrottko² , H T Grahn²  and J H van Helden¹ 

¹ Leibniz Institute for Plasma Science and Technology (INP), Felix-Hausdorff-Str. 2, 17489 Greifswald, Germany

² Paul-Drude-Institut für Festkörperelektronik, Leibniz-Institut im Forschungsverbund Berlin e. V., Hausvogteiplatz 5–7, 10117 Berlin, Germany

E-mail: jente.wubs@inp-greifswald.de

Received 14 December 2022, revised 18 January 2023

Accepted for publication 1 February 2023

Published 17 February 2023



CrossMark

Abstract

This paper describes the first implementation of terahertz (THz) quantum cascade lasers for high-resolution absorption spectroscopy on plasmas. Absolute densities of ground state atomic oxygen were directly obtained by using the fine structure transition at approximately 4.75 THz. Measurements were performed on a low-pressure capacitively coupled radio frequency oxygen discharge. The detection limit in this arrangement was found to be $2 \times 10^{13} \text{ cm}^{-3}$, while the measurement accuracy was within 5%, as demonstrated by reference measurements of a well-defined ammonia transition. The results show that the presented method is well suited to measure atomic oxygen densities, and it closes the THz gap for quantitative atomic density measurements in harsh environments such as plasmas.

Keywords: terahertz, absorption spectroscopy, quantum cascade lasers, atomic oxygen

(Some figures may appear in colour only in the online journal)

1. Introduction

Oxygen-containing plasmas are widely used in industry for a variety of applications, including etching, chemical vapour deposition, and plasma sterilisation of medical devices [1–3]. Due to its high reactivity, atomic oxygen is a highly relevant species in most of these applications. For example, it has been shown that oxygen atoms play a key role in the removal of

photoresist [4], the surface modification of polymers [5], and the deposition of metal oxide films [6]. Knowledge on the densities of oxygen atoms is crucial for the development of applications and a fundamental understanding of the chemistry in oxygen-containing plasmas. The accurate determination of absolute atomic oxygen densities is therefore of great importance.

There are several diagnostic techniques currently available to measure atomic oxygen densities. First of all, two-photon absorption laser-induced fluorescence (TALIF) is a well-established technique, although it is rather complex and expensive [7–9]. In addition, TALIF measurements are indirect, meaning that a calibration procedure is required to obtain absolute atomic oxygen densities, which involves a comparison between two-photon excitation cross sections for oxygen and xenon [10]. A second technique that has been used in the past to measure atomic oxygen densities is

³ Present address: Physikalisch-Technische Bundesanstalt, Institut Berlin, Abbestr. 2–12, 10587 Berlin, Germany.

* Author to whom any correspondence should be addressed.



Original Content from this work may be used under the terms of the [Creative Commons Attribution 4.0 licence](https://creativecommons.org/licenses/by/4.0/). Any further distribution of this work must maintain attribution to the author(s) and the title of the work, journal citation and DOI.

actinometry [11–14]. This is a relatively simple method based on optical emission spectroscopy, using e.g. the emission lines of atomic oxygen at wavelengths of approximately 777 and 844 nm, respectively. However, it relies upon the introduction of a chemical actinometer (e.g. argon), which can perturb the plasma, and an accurate modelling of excitation and relaxation processes. Other techniques for studying atomic oxygen densities in plasmas include chemical titration with NO molecules and catalytic probes [15].

As opposed to the aforementioned indirect methods, absorption spectroscopy directly provides absolute ground state densities, and the measurement accuracy depends almost exclusively on the accuracy to which the transition line strength (or, alternatively, the absorption cross section) is known. The absorption spectrum of atomic oxygen lies partially in the vacuum ultraviolet region of the electromagnetic spectrum, which is experimentally very challenging [16]. In addition, atomic oxygen has some weak transitions in the visible range, such as the forbidden $^1D_2 \leftarrow ^3P_2$ transition at approximately 630 nm; however, they only become detectable when using e.g. cavity ringdown spectroscopy (CRDS) to enhance the signal strength [17–19].

Much stronger, and therefore seemingly easier to detect, are some of the transitions between fine structure levels of the ground state. The strongest fine structure transition of ground state atomic oxygen is the $^3P_1 \leftarrow ^3P_2$ transition at approximately 63 μm , which corresponds to an energy of 0.020 eV and a frequency of approximately 4.75 THz, or, equivalently, a wavenumber of approximately 158 cm^{-1} [20]. This transition was previously not considered as an option for absorption spectroscopy measurements due to the lack of suitable radiation sources and detectors in this spectral range, i.e. the so-called terahertz (THz) gap. However, a number of powerful and efficient THz sources have been developed over the last three decades, such as THz lasers, laser-based THz sources (with THz generation by e.g. photoconductive devices or optical rectification in nonlinear crystals), and accelerator-based THz sources [21, 22]. This has led to a rapid development of science and technology based on THz radiation, including new diagnostics that are an important advancement in the field of plasma physics [23].

Among some of the most promising THz sources for absorption spectroscopy are quantum cascade lasers (QCLs). They typically have a narrow linewidth (a few MHz down to kHz), making them an excellent source for high-resolution spectroscopy [24]. The development of QCLs in the mid-infrared (MIR) in combination with their commercial availability and convenient operating conditions have turned MIR laser absorption spectroscopy into a standard plasma diagnostic technique [25, 26]. Significant progress on the development of QCLs with emission frequencies in the THz range has been made in recent years as well [27]. This allows them to be implemented as radiation sources for spectroscopic applications. So far, there are a few reports on the application of THz QCLs for absorption spectroscopy in the gas phase [28–31]. In addition, THz QCLs have been employed in astronomy and planetary science, where they are used as local oscillators in a heterodyne spectrometer for the detection of

oxygen atoms in space [32]. However, works on the application of THz QCLs for spectroscopic measurements on artificially generated plasmas do not yet exist.

Therefore, THz QCLs have recently been developed for the purpose of detecting atomic oxygen in plasmas by using the fine structure transition at approximately 4.75 THz [33, 34]. This paper reports on the first implementation of these lasers for high-resolution absorption spectroscopy, and it demonstrates the suitability of THz absorption spectroscopy as a diagnostic technique for measuring atomic oxygen densities. To this end, measurements of absolute ground state atomic oxygen densities were performed on a low-pressure capacitively coupled radio frequency (CCRF) oxygen discharge. A detailed description of the measurement procedure is given, and first results on atomic oxygen densities are presented for a variation of the applied RF power and gas pressure.

2. Experimental setup

For detecting the fine structure transition of atomic oxygen at $158.268\,741\text{ cm}^{-1}$ (i.e. 4.744 777 49 THz) [20], a tunable QCL exhibiting single-mode operation was developed based on GaAs/AlAs heterostructures. More details on the development of this QCL can be found in the work of Lü *et al* [34]. Stable laser operation could be realised in continuous-wave mode with optical output powers ranging from 1 to 8 mW at operating temperatures below 70 K. The QCL was therefore operated in a Stirling cryocooler (Ricor K535), as schematically illustrated in figure 1. The laser temperature was regulated by an additional temperature controller (Stanford Research Systems, CTC100) that was capable of a temperature control with $< 5\text{ mK}$ stability. As the laser output was very sensitive to small temperature fluctuations, such a precise temperature control was a prerequisite for measuring absorption spectra with high resolution. Tuning of the laser output across a frequency range of approximately 3 GHz was achieved by linearly ramping the input current. Continuous ramping instead of discrete stepping of the current (as was done in the work of Hübers *et al* [28]) was enabled by the stable and mode-hop-free behaviour of the used THz QCL [34]. It allowed for faster measurements with a much better spectral sampling rate (with frequency ‘steps’ down to $1 \times 10^{-7}\text{ cm}^{-1}$, i.e. 3 kHz; for reference, the frequency steps used in [28] are of the order of 1 MHz). The current was supplied by a laser driver (Wavelength Electronics, QCL1000 OEM) that was controlled by a function generator (Tektronix, AFG3022C) to provide sawtooth waveforms with a frequency of 10 Hz (or, equivalently, a period of 100 ms) and minimum and maximum current values of 480 and 600 mA, respectively. To accurately detect absorption features, even smaller tuning ranges had to be used; the reason for this will be explained in section 3.2.

The generated THz radiation was collected by a gold-coated parabolic mirror to produce a collimated beam with a diameter of $(3 \pm 1)\text{ mm}$. After passing through the object(s) of interest (e.g. an etalon, reference gas cell (RGC), or plasma reactor), the laser radiation was detected by a

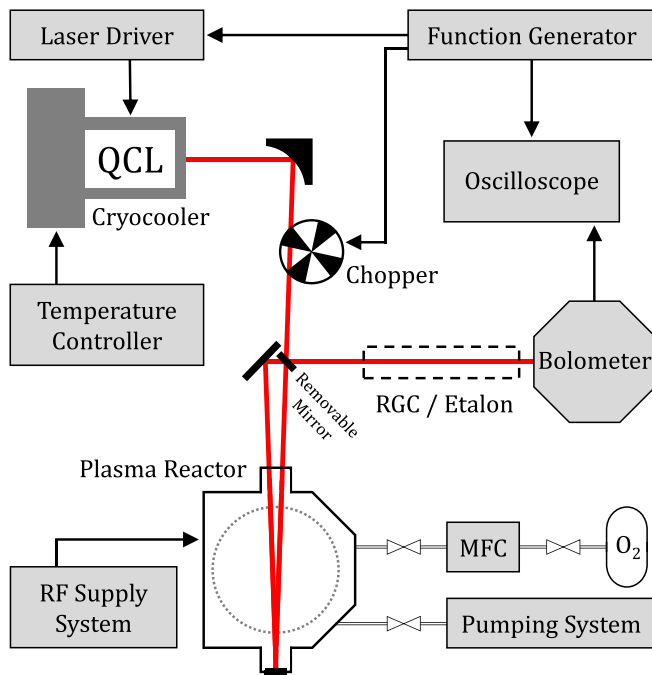


Figure 1. Schematic overview of the experimental setup for THz absorption spectroscopy. QCL: quantum cascade laser, RGC: reference gas cell, MFC: mass flow controller.

helium-cooled bolometer (Infrared Laboratories, 4.2K Bolometer). A wedged white polyethylene window in combination with an additional far-infrared filter prevented radiation above 370 cm^{-1} from reaching the detector element. Since the principle of a bolometer is based on measuring a change in temperature, the incident radiation had to be modulated to allow the bolometer to excite and relax. Therefore, a phase-locked optical chopper (New Focus, Model 3502) with a frequency of 5 Hz was used, blocking each second period of the laser output. The detected signals were recorded with a digital sampling oscilloscope (R&S, RTO 1014), and all results presented in this paper were averaged over 200 individual measurements to improve the signal-to-noise ratio.

The plasma that was investigated in this work is an asymmetric CCRF discharge generated in pure oxygen. The planar RF electrode was made of stainless steel and had a diameter of 120 mm. It was powered at 13.56 MHz by an RF generator (Advanced Energy, Cesar 133) and an automatic matching network (Advanced Energy, Navio). The applied RF power was varied between 20 and 100 W. The RF electrode was positioned at a distance of 55 mm beneath the top surface of the grounded reactor vessel, which consisted of aluminum and was cylindrically shaped, with a diameter of 240 mm and a height of 105 mm. A window made of silicon (HRFZ-Si with $> 50\%$ transmission in the THz range) allowed for the laser beam to pass through the reactor, at a height of approximately 18 mm above the RF electrode. A gold-coated mirror at the back end of the reactor reflected the laser beam back towards the entrance window, with a slight angle between the incident and reflected beam (see figure 1) to avoid having an etalon effect disturbing the signal. The effective absorption length

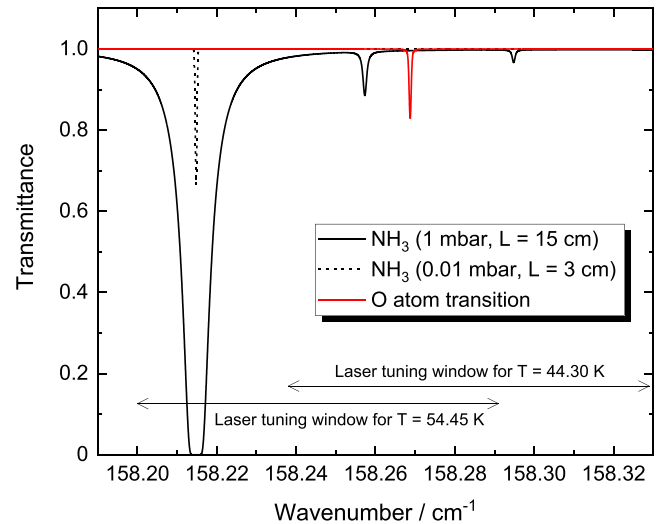


Figure 2. Simulated transmission spectra ($T = 296\text{ K}$) of ammonia and atomic oxygen from the HITRAN spectral database [36]. Laser tuning windows corresponding to laser currents between 480 and 600 mA are indicated for laser temperatures of 44.30 and 54.45 K.

was estimated to be $(84 \pm 2)\text{ cm}$ (i.e. the total length of the laser beam path within the plasma reactor), assuming that oxygen atoms are not confined by the boundaries of the visible plasma above the RF electrode but distributed throughout the entire plasma reactor. Before filling the reactor vessel with oxygen gas, it was pumped to a base pressure of $< 5 \times 10^{-4}\text{ mbar}$ by a turbopump system (Pfeiffer Balzers, TSU 062). After that, oxygen was admitted to the vessel and the pressure was adjusted to 0.7 or 1.3 mbar. The gas flow was set to 70 sccm by a mass flow controller (MKS 1179A with control unit MKS 647C) connected to an oxygen gas cylinder (Air Liquide, gas purity 99.998%).

Additionally, an etalon or RGC could be placed in the beam path, as shown in figure 1. In those cases, an additional mirror was added to the setup to shorten the optical path length and, hence, improve the signal intensity. Measurements on a silicon etalon (refractive index: 3.4175 ± 0.0003 [35]) with a length of 9 cm were performed to obtain the relation between current and (relative) wavenumber. For the measurements on RGCs, glass cells of varying length were used with silicon windows at both ends. They were filled with ammonia (NH_3) to known pressures in the range between 0.01 and 2 mbar. Ammonia was used as reference gas because it has some well-defined absorption features close to the fine structure transition of atomic oxygen, as can be seen from the simulated transmission spectra shown in figure 2. The physical constants needed to simulate these spectra (e.g. transition wavenumbers, pressure broadening coefficients, and line strengths) were obtained from the HITRAN spectral database [36]. The laser tuning windows for the two laser temperatures used in this work are indicated in figure 2 as well, for laser currents between 480 and 600 mA, where increasing the laser current corresponds to decreasing the wavenumber (tuning coefficient: $7.8 \times 10^{-4}\text{ cm}^{-1}/\text{mA}$). For most measurements, a laser temperature of 44.30 K was used, as lower operating temperatures

led to higher output powers; the higher laser temperature (54.45 K) was therefore only used to detect the ammonia transition at $158.214\,792\text{ cm}^{-1}$. Measurements of different ammonia transitions were performed to obtain information on the instrumental function and to validate the measurement procedure, thereby allowing for an accurate analysis of the measured atomic oxygen spectra.

3. Results and discussion

3.1. Spectral lines and their positions

The three ammonia transitions investigated in this work are purely rotational transitions in the ground state. An overview of these transitions, including their line positions and assignments, is given in table 1. The assignment notation used here corresponds to $\Delta J(J'', K_a'')$, where J'' and K_a'' are the lower-state quantum numbers of the $(J', K_a') \leftarrow (J'', K_a'')$ transition; J is associated with the total angular momentum and K_a with its projection along the principle axis (C3) of the ammonia molecule.

To record a spectrum that contains absorption features of both atomic oxygen and ammonia, the laser radiation passing through the plasma reactor and a RGC filled with ammonia was measured. The resulting spectrum is given in figure 3. Here, it can be seen that the rising and falling slopes of the signal are affected by the opening and closing of the optical chopper, whereas the unaffected part of the signal (i.e. when the chopper is fully open) contains the relevant spectral information. The wavenumber axis was determined from an etalon measurement and shifted according to the $R(7,5)$ -transition of $^{15}\text{NH}_3$ at $158.257\,314\text{ cm}^{-1}$, whose position is accurately known (uncertainty: $< 0.0001\text{ cm}^{-1}$) [37]. With this wavenumber axis, the fine structure transition of atomic oxygen is located at a position that matches within the margin of error with the transition wavenumber of $158.268\,741\text{ cm}^{-1}$ given in literature (uncertainty: $\approx 0.00001\text{ cm}^{-1}$) [20]. In addition, a second ammonia transition is visible in the spectrum, namely, the $aR(7,2)$ -transition of $^{14}\text{NH}_3$. It has a reported transition wavenumber of $158.294\,830\text{ cm}^{-1}$, but with a relatively large uncertainty (in the range between 0.001 and 0.01 cm^{-1}) [38]. The transition wavenumber can be determined with a much better accuracy from the spectroscopic measurements presented in this work. Its value as obtained from the spectrum in figure 3 equals $(158.2958 \pm 0.0002)\text{ cm}^{-1}$, where the indicated possible error is due to the uncertainty in the determination of the wavenumber axis. Although the focus of this paper is on the fine structure transition of atomic oxygen and this particular ammonia transition will be of no further interest, it clearly demonstrates that the emergence of high-resolution spectroscopy in the THz range is highly promising for improving the current state of knowledge on spectroscopic parameters of atoms and molecules.

The third ammonia transition that is of importance in this work is the $sR(7,3)$ -transition of $^{14}\text{NH}_3$ at $158.214\,792\text{ cm}^{-1}$ (uncertainty: $< 0.0001\text{ cm}^{-1}$) [39]. It lies outside the laser tuning window used for recording the spectrum in figure 3, but it

Table 1. Details of the investigated ammonia transitions as obtained from the HITRAN spectral database [36]. Line positions are given in cm^{-1} and line strengths at $T = 296\text{ K}$ in $\text{cm}^{-1}/(\text{molecule cm}^{-2})$.

Isotope	Line position	Line strength	Assignment
$^{14}\text{NH}_3$	158.214 792	2.828×10^{-19}	$sR(7,3)$
$^{15}\text{NH}_3$	158.257 314	5.095×10^{-22}	$R(7,5)$
$^{14}\text{NH}_3$	158.294 830	1.031×10^{-22}	$aR(7,2)$

can be reached by changing the laser temperature. This line is relatively strong (for its line strength, see table 1) and therefore ideal for characterising the broadening of spectral lineshapes.

3.2. Avoiding asymmetric effects

For examining individual lines and their spectral absorption profiles, raw spectra were converted into a transmittance T_ν or absorbance A_ν using

$$A_\nu = -\ln(I/I_0) \equiv -\ln(T_\nu), \quad (1)$$

with I the measured intensity signal and I_0 the original intensity that would have been measured without absorption. Noise and fluctuations caused I_0 to be insufficiently reproducible for it to be measured separately; therefore, it was determined by fitting a second order polynomial function to I while excluding the part affected by absorption from the fit. The resulting absorption spectrum, recorded with a laser tuning window of 120 mA and zoomed in on the $sR(7,3)$ -transition of $^{14}\text{NH}_3$ at $158.214\,792\text{ cm}^{-1}$, is given by the black curve in figure 4.

Although spectral profiles naturally have a symmetrical lineshape, the spectral lines of ammonia and atomic oxygen examined in this study all seemed to be asymmetric. This had to be a detection-related effect, presumably because the bandwidth of the bolometer was too low to correctly record the shape of the observed absorption features. To verify this assumption, the speed of the laser tuning was slowed down. To this end, the minimum and maximum current values were adapted, thereby reducing the wavenumber tuning range. The resulting spectral profiles for different laser tuning speeds are shown in figure 4, demonstrating that the same absorption line becomes more symmetric when it is recorded with a lower laser tuning speed. This confirms that the detection principle of the bolometer can induce an asymmetric deformation of the measured signals. To minimise this effect, all spectral lines were detected using the smallest possible wavenumber tuning window, i.e. the minimum and maximum laser current values were chosen such that the entire absorption feature was detected with sufficient space on both sides to be able to determine I_0 . Measurements of the $sR(7,3)$ -transition of $^{14}\text{NH}_3$ at $158.214\,792\text{ cm}^{-1}$, for example, were performed using a laser tuning window of 10 mA (or, equivalently, a laser tuning speed of 100 mA s^{-1} , due to the 100 ms measurement period), whereas a laser tuning window of 20 mA was needed for detecting the $R(7,5)$ -transition of $^{15}\text{NH}_3$ at $158.257\,314\text{ cm}^{-1}$. This corresponds to a wavenumber range of approximately 0.0078 or 0.016 cm^{-1} , respectively.

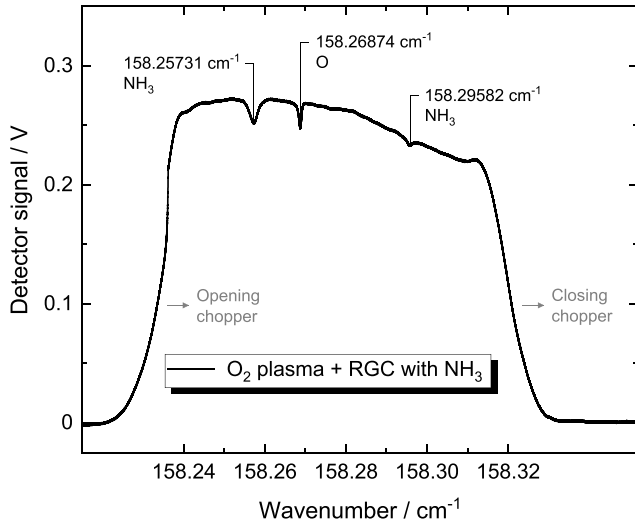


Figure 3. Raw spectrum from a simultaneous measurement of a RGC with NH_3 ($p = 2$ mbar, $L = 15$ cm) and an O_2 plasma ($p = 1.3$ mbar, $P = 30$ W), measured with a laser temperature of 44.30 K.

However, both are far too small for an etalon measurement; for reference, the distance between the fringes of the used 9 cm silicon etalon amounts to 0.0325 cm^{-1} . The measurements are therefore based on the assumption that the current-wavenumber relation derived from an etalon measurement with a 120 mA tuning window still applies for smaller tuning windows. The observation that the area under the absorbance is barely changing indicates that this is a valid assumption, since this area is determined by the ammonia density and not affected by spectral line broadening.

3.3. Broadening of spectral lineshapes

While the area under the absorbance is generally related to the density of the absorbing species, the lineshape of the spectral profile is determined by several broadening mechanisms. The relevant mechanisms behind the lineshapes of the spectral profiles presented in this work include collisional broadening, Doppler broadening, and instrumental broadening. The first two mechanisms are dictated by spectroscopic properties of the absorbing species as well as experimental conditions (i.e. the pressure and temperature of the gas sample, respectively), while the latter is governed by properties of the involved instruments (e.g. the laser linewidth) [41]. When deducing properties of a plasma from the lineshape of spectral absorption profiles, it is important to know the shape of the instrumental function. It can best be determined from a strong spectral line that can be measured at such a low pressure that the contribution from collisional broadening to the lineshape becomes negligible. Collisional broadening would typically lead to a Lorentzian lineshape with a full width at half maximum (FWHM) given by

$$\Delta\nu_L = 2\gamma p, \quad (2)$$

with p being the pressure and γ the pressure broadening coefficient, whose value can be found in literature [40]. If collisional

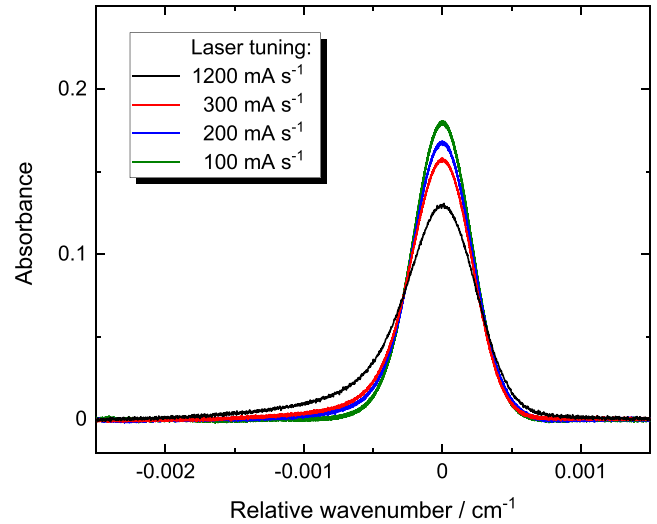


Figure 4. Comparison of the absorption spectra of a RGC with NH_3 ($p \approx 0.01$ mbar, $L = 3$ cm), showing the $sR(7,3)$ -transition of $^{14}\text{NH}_3$ at $158.214792 \text{ cm}^{-1}$, for different laser tuning speeds and a laser temperature of 54.45 K.

broadening is negligible, the only other relevant broadening mechanism, apart from instrumental broadening, is Doppler broadening. This broadening mechanism leads to a Gaussian lineshape with a FWHM of

$$\Delta\nu_D = 2\nu_0 \left(\frac{2\ln(2)k_B T}{mc^2} \right)^{1/2}, \quad (3)$$

where ν_0 is the transition wavenumber, k_B the Boltzmann constant, m the mass of the absorbing species, and c the speed of light [41]. At room temperature (i.e. 296 K), $\Delta\nu_D$ equals $4.7 \times 10^{-4} \text{ cm}^{-1}$. To determine the instrumental contribution to the broadening of spectral lineshapes, the $sR(7,3)$ -transition of $^{14}\text{NH}_3$ at $158.214792 \text{ cm}^{-1}$ was measured at a pressure of approximately 0.01 mbar using a RGC with a length of 3 cm. A Gaussian function was fitted to the recorded spectral profile, as shown in figure 5. The residual, i.e. the difference between the measured absorption profile and the fit, is included in figure 5 as well. The fit clearly demonstrates that the instrumental function has a Gaussian lineshape. The FWHM of the fit is approximately $4.9 \times 10^{-4} \text{ cm}^{-1}$, and after a simple calculation (see the inset in figure 5) it can be deduced that $\Delta\nu_{\text{inst}} = (1.4 \pm 0.6) \times 10^{-4} \text{ cm}^{-1}$. This corresponds to a laser linewidth of 4.2 MHz and is mainly caused by instabilities in the current supplied by the laser driver, which is a typical challenge for QCLs in the MIR range as well.

3.4. Validation by using a known reference gas line

According to the Beer–Lambert law, the area under a spectral absorption profile equals

$$\int_{\text{line}} A_\nu(\nu) d\nu = LnS(T), \quad (4)$$

where L is the absorption length, n the total density of the absorbing species, and $S(T)$ the line strength of the transition

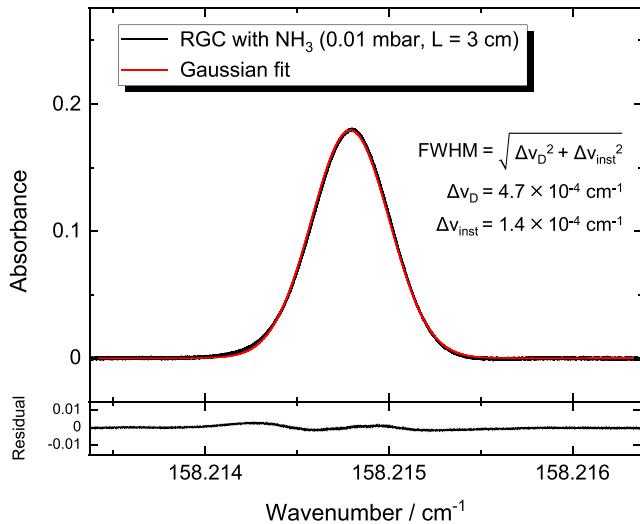


Figure 5. Spectral absorption profile of the $sR(7,3)$ -transition of $^{14}\text{NH}_3$ at $158.214792\text{ cm}^{-1}$, measured in a RGC with NH_3 ($p \approx 0.01\text{ mbar}$, $L = 3\text{ cm}$) using a laser tuning speed of 100 mA s^{-1} and a laser temperature of 54.45 K . A Gaussian function was fitted to the profile; the corresponding residual is given in the bottom part of the figure.

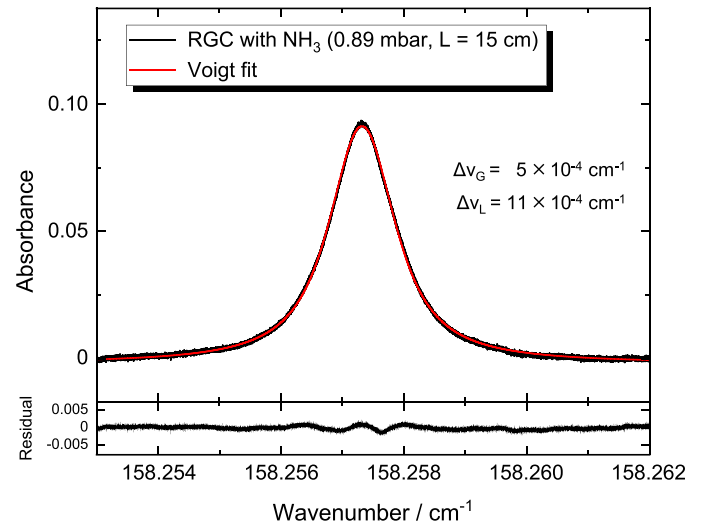


Figure 6. Spectral absorption profile of the $R(7,5)$ -transition of $^{15}\text{NH}_3$ at $158.257314\text{ cm}^{-1}$, measured in a RGC with NH_3 ($p = 0.89\text{ mbar}$, $L = 15\text{ cm}$) using a laser tuning speed of 200 mA s^{-1} and a laser temperature of 44.30 K . A Voigt function was fitted to the profile; the corresponding residual is given in the bottom part of the figure.

at temperature T [41]. In the case of reference gas measurements performed at room temperature ($T = 293\text{ K}$), the density can also be calculated from the pressure using the ideal gas law ($p = nk_B T$). Absorption measurements of a well-defined transition at a precisely known pressure can therefore serve as a means to validate the method presented in this work. Of the three examined ammonia transitions, the $R(7,5)$ -transition of $^{15}\text{NH}_3$ at $158.257314\text{ cm}^{-1}$ is most suitable for this purpose. It was investigated at a pressure of 0.89 mbar using a RGC with a length of 15 cm . To allow for an accurate comparison, the pressure in the cell was measured with high precision using frequency comb-based Fourier transform spectroscopy in the range from 3145 to 3390 cm^{-1} [42]. The result yielded by this well-established method is $p = (0.89 \pm 0.01)\text{ mbar}$.

The spectral profile of the selected ammonia transition as obtained with THz absorption spectroscopy is presented in figure 6. This absorption line is clearly broader than the one in figure 5 (note the different scaling of the wavenumber axes), as collisional broadening significantly affects the spectral lineshape at this pressure. Therefore, the spectral profile has not only a Gaussian but also a Lorentzian component, and it was fitted with a Voigt function, as can be seen in figure 6. Correctly fitting a Voigt function to the data is, however, not straightforward. In principle, the Lorentzian width can be calculated from equation (2), as both the pressure and pressure broadening coefficient are accurately known (the latter with an uncertainty in the range between 2 to 5% [40]). However, the combination of this Lorentzian width ($\Delta\nu_L = 8.0 \times 10^{-4}\text{ cm}^{-1}$) and the Gaussian contributions from Doppler and instrumental broadening (see section 3.3) is insufficient to account for the observed spectral profile with a FWHM of approximately $13 \times 10^{-4}\text{ cm}^{-1}$.

So, either $\Delta\nu_L$, $\Delta\nu_G$, or both have to be slightly larger than their computed values (see for example figure 6, where the fit has a Lorentzian width of $11 \times 10^{-4}\text{ cm}^{-1}$). The area under the fit is proportional to the pressure, and it can be derived that $p = (0.92 \pm 0.05)\text{ mbar}$, where the indicated possible error is due the uncertainty in the fitting procedure. This result is in excellent agreement with the value obtained with frequency comb-based Fourier transform spectroscopy, and, consequently, it demonstrates the accuracy of the method presented in this work.

3.5. Results on atomic oxygen densities

The atomic oxygen transition investigated in this work is the $^3\text{P}_1 \leftarrow ^3\text{P}_2$ transition at $158.268741\text{ cm}^{-1}$ between fine structure levels of the ground state. A typical example of the spectral absorption profile of this transition, obtained from measurements on a CCRF discharge in pure oxygen at a pressure of 1.3 mbar and an applied power of 30 W , is shown in figure 7, including a Gaussian fit to the profile. The W-shape of the residual, here more pronounced than in figures 5 and 6, could be attributed to plasma-induced disturbances on the signal, which did not fully disappear after averaging. Additionally, it could also be a result of averaging over inhomogeneous density and temperature distributions (as absorption spectroscopy is a line-of-sight integrated technique).

With equation (4), the area under the fit can be converted into a value for the atomic oxygen density. Here, it is worth emphasising that, when using this form of the Beer–Lambert law, the obtained density represents the total density of atomic oxygen in all three fine structure levels of the ground state (i.e. $^3\text{P}_2$, $^3\text{P}_1$ and $^3\text{P}_0$) instead of the density of atoms in

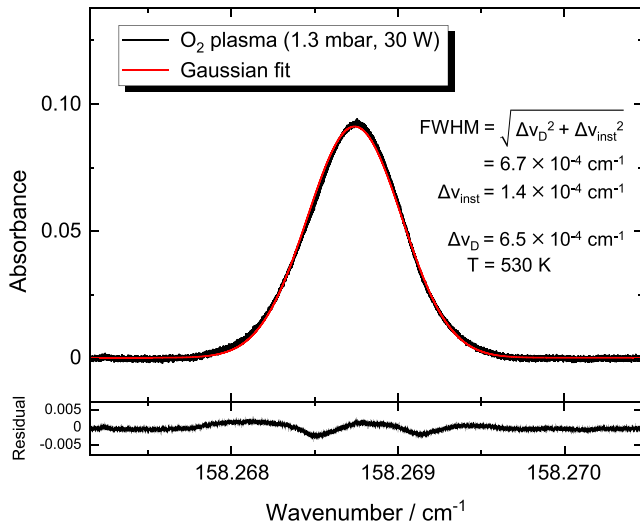


Figure 7. Spectral absorption profile of the fine structure transition of atomic oxygen at $158.268\,741\text{ cm}^{-1}$, measured in a CCRF O_2 discharge ($p = 1.3\text{ mbar}$, $P = 30\text{ W}$) using a laser tuning speed of 74 mA s^{-1} and a laser temperature of 44.30 K . A Gaussian function was fitted to the profile; the corresponding residual is given in the bottom part of the figure.

the lower energy level (i.e. $^3\text{P}_2$) only. The reason for this is that the definition of the line strength $S(T)$ is based on the assumption that the energy levels are populated according to a Boltzmann distribution [41]. The temperature dependence of the line strength follows from Boltzmann statistics and ensures a correct calculation of the total density from the lower level density. At room temperature, for example, the percentage of oxygen atoms occupying the lower level equals 74%. This factor, whose value decreases for higher temperatures, is included in the line strength to directly obtain the total atomic oxygen density. For atomic oxygen, the assumption of having a Boltzmann distribution of the energy levels can be legitimately made even at low pressure because the energy separation between the fine structure levels is very small ($\approx 0.020\text{ eV}$); therefore, few heavy-particle collisions are sufficient to establish a Boltzmann equilibrium. That the fine structure levels are indeed in thermodynamic equilibrium has been shown in [18] for an inductively coupled RF oxygen discharge at pressures more than an order of magnitude lower than those employed here. It is therefore reasonable to assume a Boltzmann distribution of the energy levels for the conditions considered in this work.

So, knowing the temperature is crucial when calculating the total density of ground state atomic oxygen from the area under the fit. The temperature is the only free parameter dictating the Doppler width (see equation (3)) and it can be derived from the Gaussian width of the fit, provided that the contribution from instrumental broadening is accurately known. The instrumental broadening has been determined from reference gas measurements (see section 3.3), and with this, the Doppler width derived from the Gaussian width of the fit is $6.5 \times 10^{-4}\text{ cm}^{-1}$ (see the inset in figure 7). However, repeating the measurements under similar circumstances led to a

slight variation in this value. This is considered to be caused by statistical errors of the measurement, possibly in combination with a slight fluctuation of plasma parameters over time. The temperature deduced from the Doppler width lies in the range between 350 and 530 K; similar temperatures can be found in other works on CCRF oxygen discharges [10, 43–45]. However, the temperature could not be determined with sufficient accuracy to observe the temperature changes that occur when adapting the applied RF power or gas pressure. Therefore, a temperature value of $T = (450 \pm 100)\text{ K}$ was used for all measurements presented in this work. It has to be noted that this temperature represents an average over the temperature distribution along the optical path of the laser beam, as absorption spectroscopy is a line-of-sight integrated technique.

The line strength of the atomic oxygen transition at $T = (450 \pm 100)\text{ K}$ can now be calculated; this was done as described in [46]. It requires knowing the value of the line strength at a reference temperature T_0 as well as the energies and statistical weights of the three fine structure levels, which can all be found in the HITRAN spectral database [36]. The line strength in HITRAN is defined at $T_0 = 296\text{ K}$ and amounts to $1.117 \times 10^{-21}\text{ cm}^{-1}/(\text{molecule cm}^{-2})$; the uncertainty in this value is, however, not given [47]. Calculating the line strength for the above-mentioned temperature T results in $S(T) = (0.80 \pm 0.17) \times 10^{-21}\text{ cm}^{-1}/(\text{molecule cm}^{-2})$, where the indicated possible error of approximately 20% accounts for the uncertainty in the temperature determination.

With this value for the line strength, the total density of ground state atomic oxygen can be calculated from the area under the fit. For the absorption profile shown in figure 7, this results in a density of $9.6 \times 10^{14}\text{ cm}^{-3}$. The total estimated possible error in the density is approximately 30%. This is mainly due to the uncertainty in the temperature determination, but also due to, among others, the uncertainty in the absorption length ($L \approx 84\text{ cm}$) and averaging over unknown density and temperature distributions. These are, however, common sources of error when working with plasmas, and it has to be noted that the technique by itself has a precision of approximately 5% only, as demonstrated by the reference gas measurements presented in section 3.4. Lastly, the limit of detection was defined as the atomic oxygen density that would correspond to an absorption profile with a peak value of three times the standard deviation of the noise level. This was determined to be $2 \times 10^{13}\text{ cm}^{-3}$.

Similar measurements of the atomic oxygen density in a CCRF oxygen discharge were performed for a variation of the applied RF power and different gas pressures. The resulting densities are shown in figure 8. They correspond to a dissociation degree of 1–2%, as can be calculated from

$$\kappa = \frac{n_{\text{O}}}{2n_{\text{O}_2}}, \quad (5)$$

where n_{O} is the atomic and n_{O_2} the molecular oxygen density; the latter follows from the ideal gas law (assuming $T_{\text{gas}} = 450\text{ K}$). Dissociation degrees of 1–2% have been reported in some other works on low-pressure CCRF oxygen

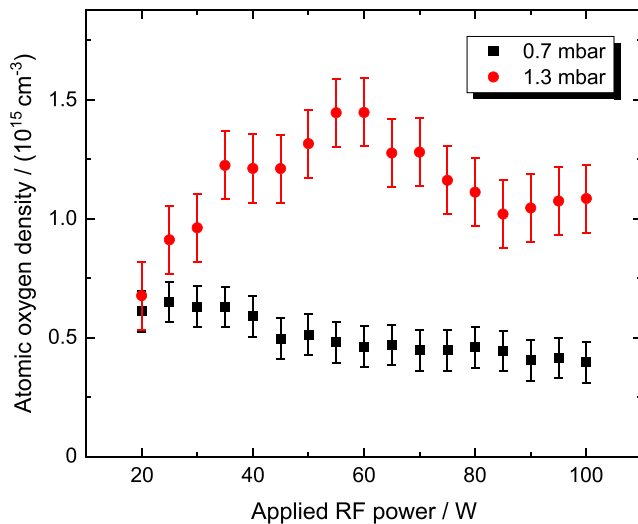


Figure 8. Comparison of atomic oxygen densities as a function of the applied RF power for different pressures. The vertical bars do not indicate the measurement error but the average spread of single data points.

discharges as well [45, 48, 49]. However, a reliable comparison with values from literature is complicated due to differences in e.g. operating conditions, reactor dimensions, or wall materials.

The vertical bars in figure 8 do not indicate the total measurement error but the average spread of single data points. Sources of error that affect all measurements equally, such as the uncertainties in the spectroscopic parameters given in the HITRAN spectral database, have thus been omitted; this allows for observing changes in the atomic oxygen density when varying the applied RF power or gas pressure. At $p = 1.3$ mbar, a clear increase in the atomic oxygen density can be observed when increasing the applied power up to approximately 60 W, whereas the atomic oxygen density is only slightly affected by the applied power at $p = 0.7$ mbar. The physio-chemical principles underlying these results will not be discussed in this paper, but a future comparison with a modelling of the plasma chemistry is expected to provide a deeper insight into the plasma-chemical behaviour. Nevertheless, the results clearly demonstrate a variation in the atomic oxygen density, as is to be expected when adapting the applied RF power or gas pressure, and it can be concluded that the presented method is well suited to investigate the influence of external parameters on the density of atomic oxygen.

4. Summary and outlook

This study demonstrated the first use of a recently developed tunable and mode-hop-free QCL for high-resolution absorption spectroscopy in the THz range. Absolute densities of ground state atomic oxygen in a low-pressure CCRF oxygen discharge were directly obtained by using the fine structure transition at 4.744 777 49 THz. The QCL was operated at temperatures below 70 K while the laser current was

continuously ramped to tune the laser frequency. The generated THz radiation was detected by a bolometer, that was found to induce an asymmetric deformation of the measured absorption features. A slowing down of the laser tuning was required to avoid this; hence, the development of faster THz detectors would be of utmost importance for THz absorption spectroscopy to become a standard diagnostic technique.

The presented method was validated by reference gas measurements of a well-defined ammonia transition, showing excellent agreement with the precisely known pressure inside the RGC. The measurement accuracy was within 5%. A second, relatively strong ammonia transition was measured at a very low pressure to obtain information on the shape of the instrumental function. This allowed for the temperature to be deduced from the measured absorption profiles of the atomic oxygen transition, resulting in $T = (450 \pm 100)$ K. Knowing the temperature was necessary to determine total densities of ground state atomic oxygen. The obtained density at a pressure of 1.3 mbar and an applied RF power of 30 W was $9.6 \times 10^{14} \text{ cm}^{-3}$, with a maximum total error of 30%. The detection limit was $2 \times 10^{13} \text{ cm}^{-3}$. Varying the applied RF power and gas pressure led to observable variations in the atomic oxygen density, and it can be concluded that the presented method is well suited to measure atomic oxygen densities in plasmas. THz absorption spectroscopy could therefore be used in the future as an alternative to existing methods for measuring atomic oxygen densities, with as main advantages the compactness of the experimental setup and the directness (i.e. no calibration procedure required) of the measurement procedure.

The experimental results presented in this paper are intended to be compared with the outcome of a plasma chemical model, with the aim of gaining further insights into the physio-chemical behaviour. In addition, future investigations will include a comparison of THz absorption spectroscopy with complementary methods, such as TALIF and CRDS. Next to this, the diagnostic capabilities of THz absorption spectroscopy are planned to be expanded to the detection of species other than atomic oxygen, such as Al atoms, OH radicals, or N^+ ions.

Data availability statement






The data that support the findings of this study are openly available at the following URL/DOI: <https://doi.org/10.34711/inptdat.672>.

Acknowledgement

This work was partially supported by the Leibniz Gemeinschaft (Grant Number: K54/2017). Furthermore, the authors would like to thank F Weichbrodt (INP) for his much appreciated technical support, I Sadiq (INP) for performing the frequency comb-based Fourier transform spectroscopy

measurements, and A J Fleisher (NIST) for a careful reading of the manuscript and fruitful discussions.

ORCID iDs

J R Wubs  <https://orcid.org/0000-0003-2035-9099>
 K-D Weltmann  <https://orcid.org/0000-0002-4161-205X>
 X Lü  <https://orcid.org/0000-0001-7169-7771>
 B Röben  <https://orcid.org/0000-0003-4356-5741>
 K Biermann  <https://orcid.org/0000-0003-4804-0784>
 L Schrottke  <https://orcid.org/0000-0002-0910-9163>
 H T Grahn  <https://orcid.org/0000-0001-5451-3950>
 J H van Helden  <https://orcid.org/0000-0001-8925-2607>

References

- [1] Hartney M A, Hess D W and Soane D S 1989 *J. Vac. Sci. Technol. B* **7** 1–13
- [2] Vesel A, Primc G, Zaplotnik R and Mozetič M 2020 *Plasma Phys. Control. Fusion* **62** 024008
- [3] Weltmann K-D, Brandenburg R, von Woedtke T, Ehlbeck J, Foest R, Stieber M and Kindel E 2008 *J. Phys. D: Appl. Phys.* **41** 194008
- [4] West A, van der Schans M, Xu C, Cooke M and Wagenaars E 2016 *Plasma Sources Sci. Technol.* **25** 02LT01
- [5] Shaw D, West A, Bredin J and Wagenaars E 2016 *Plasma Sources Sci. Technol.* **25** 065018
- [6] Yang W and Wolden C A 2006 *Thin Solid Films* **515** 1708–13
- [7] Walkup R E, Saenger K L and Selwyn G S 1986 *J. Chem. Phys.* **84** 2668–74
- [8] Niemi K, Schulz-von der Gathen V and Dobelev H F 2005 *Plasma Sources Sci. Technol.* **14** 375–86
- [9] Gazeli K, Lombardi G, Aubert X, Duluard C Y, Prasanna S and Hassouni K 2021 *Plasma* **4** 145–71
- [10] Goehlich A, Kawetzki T and Dobelev H F 1998 *J. Chem. Phys.* **108** 9362–70
- [11] Booth J P, Joubert O, Pelletier J and Sadeghi N 1991 *J. Appl. Phys.* **69** 618–26
- [12] Katsch H M, Tewes A, Quandt E, Goehlich A, Kawetzki T and Dobelev H F 2000 *J. Appl. Phys.* **88** 6232–8
- [13] Greb A, Niemi K, O'Connell D and Gans T 2014 *Appl. Phys. Lett.* **105** 234105
- [14] Steuer D, van Impel H, Gibson A R, Schulz-von der Gathen V, Böke M and Golda J 2022 *Plasma Sources Sci. Technol.* **31** 10LT01
- [15] Mozetič M, Ricard A, Babič D, Poberaj I, Levaton J, Monna V and Cvelbar U 2003 *J. Vac. Sci. Technol. A* **21** 369–74
- [16] Niemi K, O'Connell D, de Oliveira N, Joyeux D, Nahon L, Booth J P and Gans T 2013 *Appl. Phys. Lett.* **103** 034102
- [17] Hancock G, Peverall R, Ritchie G A D and Thornton L J 2007 *J. Phys. D: Appl. Phys.* **40** 4515–8
- [18] Peverall R, Rogers S D A and Ritchie G A D 2020 *Plasma Sources Sci. Technol.* **29** 045004
- [19] Rogers S D A, Bond A, Rhodes B J, Peverall R, Hancock G and Ritchie G A D 2022 *Plasma Sources Sci. Technol.* **31** 115006
- [20] Zink L R, Evenson K M, Matsushima F, Nelis T and Robinson R L 1991 *Astrophys. J.* **371** L85
- [21] Dhillon S S and Vitiello M S et al 2017 *J. Phys. D: Appl. Phys.* **50** 043001
- [22] Neu J and Schmuttenmaer C 2018 *J. Appl. Phys.* **124** 231101
- [23] Adamovich I and Agarwal S et al 2022 *J. Phys. D: Appl. Phys.* **55** 373001
- [24] Hübers H-W, Richter H and Wienold M 2019 *J. Appl. Phys.* **125** 151401
- [25] Röpcke J, Davies P B, Lang N, Rousseau A and Welzel S 2012 *J. Phys. D: Appl. Phys.* **45** 423001
- [26] Röpcke J, Davies P B, Hamann S, Hannemann M, Lang N and van Helden J-P 2016 *Photonics* **3** 45
- [27] Williams B S 2007 *Nat. Photon.* **1** 517–25
- [28] Hübers H-W, Pavlov S G, Richter H, Semenov A D, Mahler L, Tredicucci A, Beere H E and Ritchie D A 2006 *Appl. Phys. Lett.* **89** 061115
- [29] Hagelschuer T, Wienold M, Richter H, Schrottke L, Grahn H T and Hübers H-W 2017 *Opt. Express* **25** 30203–13
- [30] Wienold M, Alam T, Schrottke L, Grahn H T and Hübers H-W 2018 *Opt. Express* **26** 6692–9
- [31] D'Arco A, Rocco D, Magboo F P, Moffa C, Ventura G D, Marcelli A, Palumbo L, Mattiello L, Lupi S and Petrarca M 2022 *Opt. Express* **30** 19005–16
- [32] Richter H, Wienold M, Schrottke L, Biermann K, Grahn H T and Hübers H-W 2015 *IEEE Trans. Terahertz. Sci. Technol.* **5** 539–45
- [33] Schrottke L et al 2020 *IEEE Trans. Terahertz. Sci. Technol.* **10** 133–40
- [34] Lü X, Röben B, Biermann K, Wubs J R, Macherius U, Weltmann K D, van Helden J H, Schrottke L and Grahn H T 2023 *Semicond. Sci. Technol.* **38** 035003
- [35] Dai J, Zhang J, Zhang W and Grischkowsky D 2004 *J. Opt. Soc. Am. B* **21** 1379–86
- [36] Gordon I E et al 2022 *J. Quant. Spectrosc. Radiat. Transfer* **277** 107949
- [37] Endres C P, Schlemmer S, Schilke P, Stutzki J and Müller H S 2016 *J. Mol. Spectrosc.* **327** 95–104
- [38] Down M J, Hill C, Yurchenko S N, Tennyson J, Brown L R and Kleiner I 2013 *J. Quant. Spectrosc. Radiat. Transfer* **130** 260–72
- [39] Pearson J 2000 private communication: Rotational, $\nu_2 - \nu_2$, and ν_2 -ground state prediction
- [40] Nemtchinov V, Sung K and Varanasi P 2004 *J. Quant. Spectrosc. Radiat. Transfer* **83** 243–65
- [41] Reuter S, Sousa J S, Stancu G D and van Helden J-P 2015 *Plasma Sources Sci. Technol.* **24** 054001
- [42] Lang N, Puth A, Kowzan G, Hamann S, Röpcke J, Masłowski P and van Helden J H 2018 Spectroscopic investigations of plasma nitrocarburizing processes with a mid-infrared frequency comb *High-Brightness Sources and Light-Driven Interactions* (Optica Publishing Group) p MW4C.3
- [43] Gomez S, Steen P G and Graham W G 2002 *Appl. Phys. Lett.* **81** 19–21
- [44] Geigl M, Peters S, Gabriel O, Krames B and Meichsner J 2005 *Contrib. Plasma Phys.* **45** 369–77
- [45] Tsutsumi T, Greb A, Gibson A R, Hori M, O'Connell D and Gans T 2017 *J. Appl. Phys.* **121** 143301
- [46] Šimečková M, Jacquemart D, Rothman L, Gamache R and Goldman A 2006 *J. Quant. Spectrosc. Radiat. Transfer* **98** 130–55
- [47] Pickett H M, Poynter R L, Cohen E A, Delitsky M L, Pearson J C and Müller H S P 1998 *J. Quant. Spectrosc. Radiat. Transfer* **60** 883–90
- [48] Morscheidt W, Hassouni K, Bauduin N, Arefi-Khonsari F and Amouroux J 2003 *Plasma Chem. Plasma Process.* **23** 117–40
- [49] Shibata M, Nakano N and Makabe T 1996 *J. Appl. Phys.* **80** 6142–7